

How are quantum eigenfunctions of hydrogen atom related to its classical elliptic orbits?

Yi-Xuan Yin(殷艺轩), Tian-Tian Wang(王天天), and Biao Wu(吴飙)
Citation: Chin. Phys. B, 2026, 35 (**5**): 050301. DOI: 10.1088/1674-1056/ae3303
http://cpb.iphy.ac.cn; http://iopscience.iop.org/cpb

What follows is a list of articles you may be interested in

Estimating quantum coherence using limited quantum resources

Bin Zou(邹斌), Kai Wu(吴凯), and Zhihua Chen(陈芝花)
Chin. Phys. B, 2026, 35 (**3**): 030301. DOI: 10.1088/1674-1056/adfb56

Control of the Liouvillian gap in the finite open quantum system

Kai-Li Li(李凯丽), Yan-Sheng Liu(刘延盛), and Xi-Zheng Zhang(张禧征)
Chin. Phys. B, 2026, 35 (**1**): 010306. DOI: 10.1088/1674-1056/adeb60

Multicast-oriented key provision in hybrid DV/CV multi-domain quantum networks

Xinyu Chen(陈欣宇), Yuan Cao(曹原), Yuxiang Lu(陆宇翔), Yue Chen(陈越), Kunpeng Zheng(郑昆朋), Xiaosong Yu(郁小松), Yongli Zhao(赵永利), Jie Zhang(张杰), and Qin Wang(王琴)
Chin. Phys. B, 2025, 34 (**9**): 090301. DOI: 10.1088/1674-1056/adecf8

Witnessing the distribution of sources in quantum networks via hierarchical nonlocality

Shu-Yuan Yang(杨舒媛), Jin-Chuan Hou(侯晋川), and Kan He(贺衎)
Chin. Phys. B, 2025, 34 (**6**): 060303. DOI: 10.1088/1674-1056/add507

Electronic and magnetic properties of semihydrogenated, fully hydrogenated monolayer and bilayer MoN_2 sheets

Yan-Chao She(佘彦超), Zhao Wei(魏昭), Kai-Wu Luo(罗开武), Yong Li(李勇), Yun Zhang(张云), Wei-Xi Zhang(张蔚曦)
Chin. Phys. B, 2018, 27 (**6**): 060306. DOI: 10.1088/1674-1056/27/6/060306

How are quantum eigenfunctions of hydrogen atom related to its classical elliptic orbits?

Yi-Xuan Yin(殷艺轩)[1], Tian-Tian Wang(王天天)[1], and Biao Wu(吴飙)[1,2,3,†]

[1] *International Center for Quantum Materials, School of Physics, Peking University, Beijing* 100871, *China*
[2] *Wilczek Quantum Center, Shanghai Institute for Advanced Studies, Shanghai* 201315, *China*
[3] *Hefei National Laboratory, Hefei* 230088, *China*

(Received 20 October 2025; revised manuscript received 23 December 2025; accepted manuscript online 4 January 2026)

We show that a highly-excited energy eigenfunction $\psi_{nlm}(\boldsymbol{r})$ of hydrogen atom can be approximated as an equal-weight superposition of classical elliptic orbits with energy E_n and angular momentum $L=\sqrt{l(l+1)}\hbar$, and z component of angular momentum $L_z=m\hbar$. This correspondence is established by comparing the quantum probability distribution $|\psi_{nlm}(\boldsymbol{r})|^2$ and the classical probability distribution $p_{\rm c}(\boldsymbol{r})$ of an ensemble of such orbits. This finding illustrates a general principle: in the semi-classical limit, an energy eigenstate of a quantum system is in general reduced to a collection of classical orbits, rather than a single classical orbit.

Keywords: hydrogen, energy eigenfunction, invariant distribution, semiclassical limit

PACS: 03.65.–w, 03.65.Sq

DOI: 10.1088/1674-1056/ae3303 **CSTR:** 32038.14.CPB.ae3303

1. Introduction

Classical mechanics is an approximation of quantum mechanics in the limit of large quantum numbers or, equivalently, as the Planck constant $\hbar$ approaches zero. This quantum-classical correspondence is often illustrated in textbooks with one dimensional harmonic oscillator[1,2] by comparing the probability density $|\psi_n(x)|^2$ of an energy eigenfunction to the probability density of the corresponding classical orbit, as shown in Fig. 1.

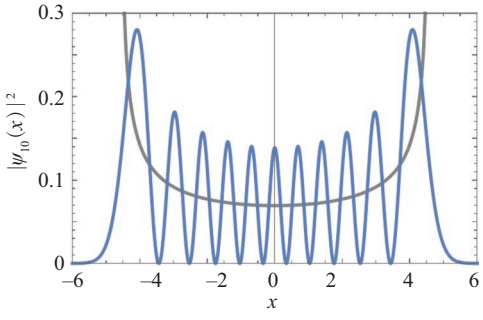


Fig. 1. Probability density of a harmonic oscillator. Blue line is the quantum probability density for the 10th energy eigenstate; the gray line is the corresponding classical probability density. The unit of x is $\sqrt{m\omega/\hbar}$, where m and ω are the mass and frequency of the oscillator, respectively.

However, this example may be misleading, as it suggests a one-to-one correspondence between a quantum energy eigenfunction and a single classical orbit. In reality, for systems with multiple degrees of freedom, a highly excited energy eigenfunction corresponds to an ensemble of classical orbits. More precisely, in the semiclassical limit $\hbar\to 0$, an energy eigenfunction is reduced to a superposition of many different classical orbits, which share the same energy but may differ in other dynamical variables. Such a superposition forms a distribution in classical phase space, which is invariant under classical evolution.[3–5]

In this work, we employ the hydrogen atom as a paradigmatic example to elucidate the general quantum-classical correspondence. Specifically, we demonstrate that a highly excited eigenstate $\psi_{n,l,m}(\boldsymbol{r})$ can be interpreted as an equal-weight superposition of all possible classical elliptic orbits with energy $E=E_n$, angular momentum $L=\sqrt{l(l+1)}\hbar$, and z-component of angular momentum $L_z=m\hbar$. We are able to compute the probability density for the ensemble of superposed elliptic orbits and compare it the quantum probability density $|\psi_{nlm}(\boldsymbol{r})|^2$. There is remarkable agreement as seen in Fig. 2.

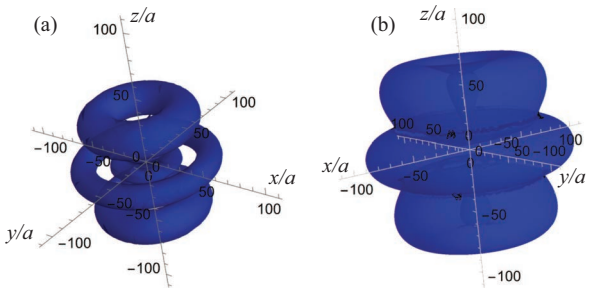


Fig. 2. Comparisons of the quantum and classical probability densities: (a) the surface where the quantum probability is $|\psi_{nlm}|^2=10^{-5}$ m^3 with $n=6$, $l=4$, and $m=2$; (b) the surface where the classical probability divided by $\sin\theta$ is 10^{-5} m^3. In the figure, a is the Bohr radius.

For hydrogen atom, the necessity of this ensemble representation for an eigenfunction $\psi_{nlm}(\boldsymbol{r})$, as opposed to a single-orbit correspondence, reflects that the three good quantum

†Corresponding author. E-mail: wubiao@pku.edu.cn

© 2026 Chinese Physical Society and IOP Publishing Ltd. All rights, including for text and data mining, AI training, and similar technologies, are reserved.

number n,l,m can not completely specify a single classical orbit.

In addition, the quantum-classical correspondence established here justifies the approximation of a quantum state of electron with classical orbits or classical ensemble distribution, which is often used in the study of ionization of atoms in strong fields.[6–9]

The rest of this article is arranged as follows: Section 2 introduces the quantum probability density as described in standard quantum physics textbooks. Section 3 derives the classical probability density, followed by a comparison of the quantum and classical results in Section 4. The overall findings are discussed in Section 5, and the Appendix addresses singularities with the quantum-classical correspondence established in this work.

2. Quantum probability density

The quantum solutions for the hydrogen atom are well-established. For completeness and to introduce notations, we briefly review them here. The energy eigenfunction ψ of the hydrogen atom satisfies the following time-independent Schrödinger equation:

$$-\frac{\hbar^2}{2m_e}\nabla^2\psi(\boldsymbol{r})+V(r)\psi(\boldsymbol{r})=E\psi(\boldsymbol{r}), \tag{1}$$

where m_e is the mass of the electron (the mass of proton is approximated as infinite) and $V(r)$ is the Coulomb potential

$$V(r)=-\frac{q^2}{4\pi\varepsilon_0 r}. \tag{2}$$

Here q is the charge of the electron. The solutions of this equation are well-known and can be found in standard textbooks.[10] In the spherical coordinates, they can be expressed as:

$$\psi_{nlm}(r,\theta,\phi)=R_{nl}(r)\mathrm{Y}_l^m(\theta,\phi), \tag{3}$$

where

$$R_{nl}(r)=\sqrt{\left(\frac{2}{na}\right)^3\frac{(n-l-1)!}{2n(n+l)!}}\left(\frac{2r}{na}\right)^l \mathrm{e}^{-r/na}L_{n-l-1}^{2l+1}\left(\frac{2r}{na}\right), \tag{4}$$

$$\mathrm{Y}_l^m(\theta,\phi)=\sqrt{\frac{2l+1}{4\pi}\frac{(l-m)!}{(l+m)!}}\,\mathrm{e}^{\mathrm{i}m\phi}\,\mathrm{P}_l^m(\cos\theta). \tag{5}$$

Here n is an integer, l is an integer satisfying $0\le l\le n-1$, m is an integer satisfying $-l\le m\le l$, and a is the Bohr radius and is given by

$$a=\frac{4\pi\varepsilon_0\hbar^2}{m_e q^2}. \tag{6}$$

For the eigenfunction ψ_{nlm}, the corresponding eigenenergy is

$$E_n=-\frac{m_e q^4}{32\pi^2\varepsilon_0^2\hbar^2 n^2}=-\frac{\hbar^2}{2m_e a^2 n^2}, \tag{7}$$

the angular momentum is $L=\sqrt{l(l+1)}\hbar$, and its z component is $L_z=m\hbar$.

In the WKB approximation, the angular momentum is chosen as $L=(l+1/2)\hbar$.[11] Here we mostly consider the situation with large l, which means the difference between $\sqrt{l(l+1)}$ and $l+1/2$ could be neglected.

We are interested in the classical counterpart of the quantum probability density $|\psi_{nlm}(r,\theta,\phi)|^2$ in the semiclassical limit $\hbar\to 0$ or, equivalently, the limit of $n\to\infty$. For the one-dimensional harmonic oscillator, in such a limit, the quantum probability distribution for an energy eigenfunction corresponds to the probability density of a single classical periodic orbit as shown in Fig. 1. This is actually true for any time-independent one-dimensional system: one eigenfunction corresponds to a single classical orbit.

However, for a general system with two or three dimensions, this assertion is not accurate. Consider the case of zero angular momentum, i.e., $l=0$. In this case, the eigenfunction $\psi_{n00}(r)$ of hydrogen atom is spherically symmetric. In contrast, the classical orbit in this case is a straight line, bearing no resemblance to the quantum state $\psi_{n00}(r)$ at all.

To reconcile this discrepancy, we note that the three good quantum numbers n, $l=m=0$ in the eigenfunction $\psi_{n00}(r)$ do not completely determine the classical orbit as the direction of the classical orbit remains unspecified. As shown in Fig. 3(a), all the straight lines inside a sphere, whose radius is determined by E_n, are possible classical orbits corresponding to the eigenfunction $\psi_{n00}(r)$.

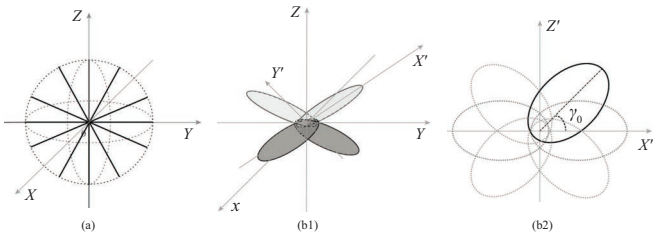


Fig. 3. Classical orbits of hydrogen atom. The origin of the coordinates is the position of proton. (a) In the special case of zero angular momentum $l=0$, the classical orbits are straight lines orientated in all possible directions. These orbits collectively fill a spherical region, reflecting that the corresponding eigenstates are s-waves. The radius of this sphere is determined by the eigen-energy E_n. (b) For non-zero angular momentum $l\neq 0$, the classical orbits for a quantum eigenstate $\psi_{nlm}(\boldsymbol{r})$ are ellipses, which can be divided into two groups: (i) the ellipses that can be transformed into each other rotating around the z axis and reflecting off the XY plane; (ii) all the ellipses that rotate around the focus of proton in the orbital plane, which is perpendicular to the angular momentum $\boldsymbol{L}$. For convenience, the $X'Y'$ coordinate system is set up in the orbital plane. The shape and size of the ellipses are determined by quantum number n and l, the orientation of the ellipses relative to the Z axis is determined by l and m.

When the angular momentum is non-zero, $l\neq 0$, the classical orbit is elliptical. Similarly, these ellipses are not completely specified by the three good quantum numbers n,l,m. The size and shape of the ellipses (the major and minor axes) are determined by n,l, while the angle between the ellipse plane and the Z axis is determined by l,m. As shown in Fig. 3(b1), when an ellipse rotates around the Z axis or gets

reflected with respect to the XY plane, its corresponding quantum numbers n,l,m remain unchanged. Moreover, as shown in Fig. 3(b2), if an ellipse rotates in its plane around the focus (where the proton is), its corresponding quantum numbers n,l,m do not change, either. All these ellipses in Figs. 3(b1) and 3(b2) correspond to the same n,l,m and form an ensemble.

As we will see, the quantum eigenfunction $\psi_{nlm}(\boldsymbol{r})$ corresponds to such an ensemble classical orbits. We will compute the classical probability density $p_{\rm c}(\boldsymbol{r})$ for such an ensemble, comparing it to the quantum quantum probability density $|\psi_{nlm}(\boldsymbol{r})|^2$. We find that in the semiclassical limit, these two densities agree with each other very well. Specifically, we will compare the quantum radial probability density $p_{\rm q}(r)=|R_{nl}(r)|^2$ and its angular probability density $p_{\rm q}(\theta)=|{\rm Y}_l^m(\theta,\phi)|^2$ to their classical counterparts, respectively.

3. Classical probability density

For a typical elliptical orbit, its standard form is given by[12]

$$r(t)=\frac{p}{1-\varepsilon\cos\gamma'(t)}, \tag{8}$$

where the parameters p and ε are determined by the energy E and angular momentum L of the orbit. The angle $\gamma'=\gamma-\gamma_0$ is illustrated in Fig. 4, where we have set up a coordinate system for an elliptical orbit. The position of proton is the origin O of the axes and thus is a focus of the ellipse, A is the position of electron at time t, $\boldsymbol{L}$ is the angular momentum vector that is perpendicular to the the orbital plane, and θ is angle between OA and the Z axis. For convenience of discussion, we set up a two-dimensional (2D) coordinate system $X'Y'$ in the orbital plane, whose origin is also O. The X' axis is set up such that it lies in the plane defined by $\boldsymbol{L}$ and the z axis. γ and γ_0 are the angles of OA and the major axis with respect to the X' axis. We pick a point B on the X' axis such that AB is perpendicular to the X' axis; similarly, C is a point on the Z axis such that AC is perpendicular to the z axis.

For a hydrogen atom in the eigenfunction $\psi_{nlm}(\boldsymbol{r})$, both its angular momentum and energy have definite values: $L=\sqrt{l(l+1)}\hbar$ and

$$E_n=-\frac{\hbar^2}{2m_{\rm e}a^2n^2}=\frac{1}{2}m_{\rm e}v^2-\frac{q^2}{4\pi\varepsilon_0 r}, \tag{9}$$

where v is the electron's speed. A classical orbit corresponding to this eigenfunction shares the same energy E_n and angular momentum L. Using the standard definition,[12] we can obtain the semilatus rectum $p=a\ell^2$ and the eccentricity

$$\varepsilon=\sqrt{1-\frac{\ell^2}{n^2}}, \tag{10}$$

where $\ell^2=l(l+1)$. For the eigenfunction $\psi_{nlm}(\boldsymbol{r})$, the Z component of angular momentum is also definite with $L_z=m\hbar$. This value of L_z fixes the angle α between the Z axis and the angular momentum vector $\boldsymbol{L}$, as shown in Fig. 4.

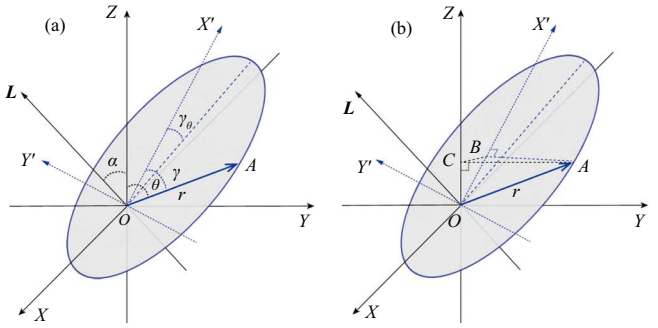


Fig. 4. One elliptic orbit in a coordinate system where the origin is the position of proton. $\boldsymbol{L}$ is the angular momentum vector. A is a point on the elliptic orbit. All the blue lines lie in the plane of the elliptic orbit. (a) α is the angle between $\boldsymbol{L}$ and the Z axis, and θ is the angle between OA and the Z axis. $X'Y'$ is a two-dimensional coordinate system in the plane of elliptic orbit. The X' axis, Z axis, and $\boldsymbol{L}$ lie in the same plane. γ_0 is the angle between the major axis of the ellipse and the X'-axis, and γ is the angle between OA and the X' axis. (b) B is a point on the X' axis, and C is a point on the Z axis. Their positions are chosen so that triangle ABC is perpendicular to the Z axis.

As already mentioned above, these three quantities E_n, L, and L_z, specified by the quantum numbers n,l,m, respectively, along with the position of the proton do not uniquely determine the elliptic orbits. Two additional parameters, L_x (or L_y) and γ_0, are needed. Shown in Fig. 3(b1) are four such orbits sharing identical E_n, L, and L_z values with $\gamma_0=0$ but different L_x; the ellipses in Fig. 3(b2) have the same values of E_n, L, L_z, and L_x with different γ_0. Due to the spherical symmetry of the hydrogen atom, it is natural to interpret the eigenfunction $\psi_{nlm}(\boldsymbol{r})$ as an equal-weight superposition of all these classical orbits with the same E_n, L, and L_z but different L_x and γ_0. We will calculate the probability densities for this ensemble, and compare them to the quantum counterparts, finding excellent agreement.

The elliptic orbit is closed and periodic. For a closed classical orbit $s(t)$ with period T (i.e., $s(0)=s(T)$), the probability $p_{\rm c}(s)$ of finding the classical particle between $s(t)$ and $s(t+\delta t)$ is defined as

$$p_{\rm c}(s)\delta s\propto\frac{\delta t}{T}=\frac{\delta s}{vT}, \tag{11}$$

where $\delta s=s(t+\delta t)-s(t)$ and v is the speed of the particle at $s(t)$. It is evident that $p_{\rm c}$ diverges at $s(t)$, where v is zero. This approach has been employed to calculate the classical probability density of a harmonic oscillator, as depicted by the gray line in Fig. 1, which diverges at the two end points of the oscillations. We will adopt this method to compute the classical radial probability density $p_{\rm c}(r)$ and angular probability density $p_{\rm c}(\theta)$, and compare them to their quantum counterparts. All the classical orbits in the classical ensemble corresponding to the eigenfunction $\psi_{nlm}(\boldsymbol{r})$ have the same period,

$$T=2\pi\frac{m_{\rm e}a^2n^3}{\hbar}, \tag{12}$$

which will be used in our calculations.

3.1. Radial probability density

We first consider the special case of zero angular momentum, $l = 0$, for two reasons: (i) to use this simplest case to illustrate how to compute the classical probability density; (ii) this special case cannot be obtained by taking the limit $l \to 0$ from the result of $l \neq 0$. In this case, as shown in Fig. 3(a), the orbits consist of all the straight lines through the center inside a sphere, whose radius is determined by the energy E_n. We focus on one of the straight lines and use r, the distance to the center, as the coordinate for this one dimensional motion. So, the velocity is given by $v = \mathrm{d}r/\mathrm{d}t$. Using Eq. (9), we find that the time the electron spends between radial distance between r and $r + \mathrm{d}r$ is

$$\mathrm{d}t = 2\frac{\mathrm{d}r}{v} = 2\frac{m_\mathrm{e}\,\mathrm{d}r}{\hbar\sqrt{2/ar - 1/n^2a^2}}. \tag{13}$$

Here the factor of 2 accounts for the electron passing through a specific radius r twice per period. Since the probability between r and $r + \mathrm{d}r$ is defined as $p_\mathrm{c}(r)\,\mathrm{d}r = \mathrm{d}t/T$, we have the probability density $p_\mathrm{c}(r)$ as

$$p_\mathrm{c}(r) = \frac{1}{\pi n^3 a\sqrt{2/\tilde{r} - 1/n^2}}, \tag{14}$$

where $\tilde{r} = r/a$. This classical density diverges at $\tilde{r} = 2n^2$, the farthest point away from the center where the electron has zero velocity.

Note that, to be precise, for a single orbit, the above density should be written as $p_\mathrm{c}(r)\delta(\theta - \theta_0)\delta(\phi - \phi_0)$, where θ_0 and ϕ_0 specify the direction of the motion. Since the density $p_\mathrm{c}(r)$ is independent of the direction, the radial probability density for the ensemble of all the possible orbits with equal weight, i.e., the sphere in Fig. 3(a), should be just $p_\mathrm{c}(r)$. This shows that we can obtain the classical probability density by focusing just on a single orbit. Other cases are similar. As a result, for brevity, in the following computation, we will not distinguish the difference between the probability density for a single orbit and the density for the ensemble.

We now consider the case where the angular momentum is not zero ($l \neq 0$). In this case, the distance that the electron moves from r to $r + \mathrm{d}r$ is

$$\mathrm{d}s = \sqrt{(\mathrm{d}r)^2 + (r\mathrm{d}\gamma)^2}\,. \tag{15}$$

Using Eq. (8), we find that

$$\mathrm{d}s = \mathrm{d}r\sqrt{1 + \frac{a^2\ell^4}{r^2\left[1 - \ell^2/n^2 - \left(1 - a\ell^2/r\right)^2\right]}}. \tag{16}$$

The time that the electron spends in the range from r to $r + \mathrm{d}r$ is $\mathrm{d}t = \mathrm{d}s/v$. Therefore, the probability density at r is

$$p_\mathrm{c}(r) = 2\frac{\mathrm{d}t}{T\,\mathrm{d}r}. \tag{17}$$

The factor of 2 here accounts for the electron passing through a specific r twice per period. Combining these results, we obtain

$$p_\mathrm{c}(r) = \frac{\sqrt{1 + \frac{\ell^4}{\tilde{r}^2\left[1 - \ell^2/n^2 - \left(1 - \ell^2/\tilde{r}\right)^2\right]}}}{\pi n^3 a\sqrt{2/\tilde{r} - 1/n^2}}. \tag{18}$$

Interestingly, this result does not reduce to Eq. (14), the result for $l = 0$, when we take the limit of $l \to 0$. When $l \neq 0$, the classical orbit is elliptical and has two points where the radial velocity vanishes, leading to divergent radial probabilities. This is evident in the above equation, which has two singular points: $r_1/a = 2\ell^2/(1 - \varepsilon)$ and $r_2/a = \ell^2/(1 + \varepsilon)$. These two singular points always exist no matter how small the angular momentum is as long as it is not zero. In contrast, the probability density $p_\mathrm{c}(r)$ has only one singular point for $l = 0$.

3.2. Angular probability density

The classical angular probability density $p_\mathrm{c}(\theta)$ can be similarly defined as:

$$p_\mathrm{c}(\theta)d\theta = \frac{\mathrm{d}t}{T} = 2\frac{\mathrm{d}s}{vT}. \tag{19}$$

The factor of 2 is included for the same reason as before. With Eq. (8), it is clear that the relation in Eq. (19) can be re-written as

$$p_\mathrm{c}(\theta)\,\mathrm{d}\theta = 2p(\gamma)\,\mathrm{d}\gamma, \tag{20}$$

where $p(\gamma)$ is the probability density in terms of γ.

To find $p(\gamma)$, we first consider the situation where $\boldsymbol{L}$ is fixed. In this case, as shown in Fig. 3(b2), all the ellipses corresponding to a given eigenfunction $\psi_{nlm}(\boldsymbol{r})$ lie in the orbital plane $x'y'$ that is perpendicular to $\boldsymbol{L}$, and these ellipses have different angle γ_0, which is indicated in Figs. 3(b2) and 4. As we average over all these ellipses, we will clearly get a uniform distribution, that is, $p(\gamma) = 1/(2\pi)$. As this result is independent of the direction $\boldsymbol{L}$, we will get the same result when we average all the ellipses with different $\boldsymbol{L}$, that is,

$$p_\mathrm{c}(\theta)\,\mathrm{d}\theta = \frac{1}{\pi}\mathrm{d}\gamma. \tag{21}$$

The remaining task is to find $\mathrm{d}\gamma/\mathrm{d}\theta$.

We use Fig. 4(b), where three additional lines AB, AC, and BC are drawn, to find the relation between θ and γ. These lines are drawn so that ΔABC is perpendicular to the Z axis. This immediately implies that OC$\perp$AC. Therefore, we have $d_\mathrm{OC} = d_\mathrm{OA}\cos\theta$, where d_OC and d_OA denote the lengths of OC and OA, respectively.

On the other hand, as AB perpendicular to both the Z axis and $\boldsymbol{L}$, AB is also perpendicular to the X' axis. This gives us another relation between d_OC and d_OA: $d_\mathrm{OC} = d_\mathrm{OB}\sin\alpha = d_\mathrm{OA}\cos\gamma\sin\alpha$. Combining the two relations, we eventually have

$$\cos\theta = \cos\gamma\sin\alpha, \tag{22}$$

a relation between γ and θ. As α is the angle between the angular momentum vector $\boldsymbol{L}$ and the z-axis, we have

$$\cos\alpha = \frac{L_z}{L} = \frac{m}{\ell}. \tag{23}$$

At the end we obtain

$$\mathrm{d}\gamma = \frac{\sin\theta}{\sqrt{\sin^2\theta - m^2/\ell^2}}\mathrm{d}\theta. \tag{24}$$

With Eq. (21), this leads to the classical angular probability density

$$p_{\mathrm{c}}(\theta) = \frac{\sin\theta}{\pi\sqrt{\sin^2\theta - m^2/\ell^2}} = \frac{\sin\theta}{\pi\sqrt{\sin^2\theta - \cos^2\alpha}}, \tag{25}$$

which diverges at two points $\theta = \pi/2 \pm \alpha$.

We note that the derivation leading to the above angular probability density is independent of the form of the interaction $V(r)$ between the particle and the center. Our argument that $p(\gamma) = 1/(2\pi)$ have not used any property of ellipse. In deriving Eq. (24), no properties of ellipse are used, either. In other words, we would get the same angular distribution even if the interaction between electron and proton is harmonic, i.e., $V(r) \propto r^2$. This is of course consistent with the result in quantum mechanics, where the angular wavefunction $\mathrm{Y}_l^m(\theta,\phi)$ is independent of the form of $V(r)$.

4. Comparison between quantum and classical results

In the semiclassical limit $n \to \infty$, we expect that the quantum probability densities converge to their classical counterparts. However, this comparison requires careful consideration of how the limit is taken. The classical probability densities are derived from an ensemble of orbits sharing identical eccentricity eccentricity ε and inclination α. For a given eigenfunction $\psi_{nlm}(\boldsymbol{r})$, the eccentricity ε is given by Eq. (10) and the inclination is determined by $\cos\alpha = m/\ell$ (see Fig. 4). To maintain physical consistency when taking $n \to \infty$, we must preserve both ε and α across eigenfunctions with different n. This requires: keeping the ratio l/n constant (fixing eccentricity) and maintaining m/l constant for $l \neq 0$ (fixing inclination). For example, with fixed ratios $l/n = 1/2$ and $l/m = 1/2$, we examine and compare the sequence of eigenfunctions $\psi_{n,n/2,n/4}(\boldsymbol{r})$ as n increases. This constrained limiting procedure ensures meaningful quantum-classical comparison and guarantees that the quantum probability densities properly converge to the classical ensemble results.

4.1. The radial probability

The quantum radial probability density for hydrogen atom is given by $p_{\mathrm{q}}(r) = |R_{nl}(r)|^2 r^2$. To obtain dimensionless probability densities, we re-define $p_{\mathrm{c}}(r)$ and $p_{\mathrm{q}}(r)$ as $p_{\mathrm{c}}(\tilde{r}) = p_{\mathrm{c}}(r)a$ and $p_{\mathrm{q}}(\tilde{r}) = p_{\mathrm{q}}(r)a$. Figure 5 compares the quantum and classical probability densities for the case $l = 0$. While the quantum probability oscillates with r, its overall trend aligns with its classical counterpart, and the agreement becomes better as the quantum number n increases. When we plot twice the classical probability density, $2p_{\mathrm{c}}(\tilde{r})$ (dashed lines), they almost perfectly envelop the quantum oscillations (blue lines). This indicates that the quantum probabilities oscillate around the classical results. If we were to smooth out these oscillations, the quantum and classical results would match almost perfectly for large n.

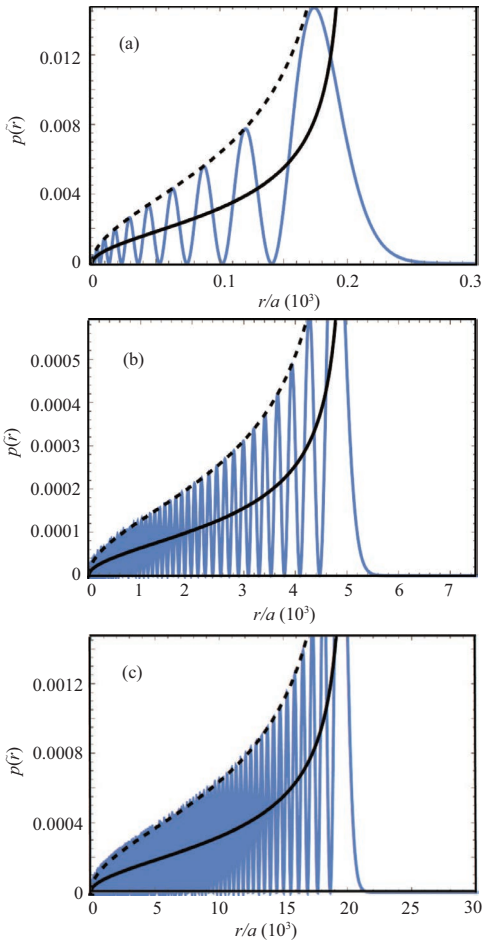


Fig. 5. The radial probability density of the hydrogen atom for the case of zero angular momentum ($l = 0$): (a) $n = 10$, $l = 0$; (b) $n = 50$, $l = 0$; (c) $n = 100$, $l = 0$. The blue lines are quantum results $p_{\mathrm{q}}(\tilde{r})$, the black solid lines are classical results $p_{\mathrm{c}}(\tilde{r})$, and the dashed lines are doubled classical results $2p_{\mathrm{c}}(\tilde{r})$.

At $r_{\mathrm{c}} = 2n^2a$, the classical electron has zero velocity, leading to divergence at this point. However, since the classical electron cannot move beyond r_{c}, its probability density immediately drops to zero for $r > r_{\mathrm{c}}$. This abrupt cutoff is well-represented by the quantum curves, which exhibit a sharp decline beyond r_{c}. Moreover, this decline becomes steeper as n increases.

Figure 6 presents a comparison of the radial probability densities for the case of non-zero angular momentum ($l \neq 0$). As we discussed at the beginning of this section, for a meaningful comparison, we must keep the ratio l/n constant as n

becomes larger. As evident from Fig. 6, there is a strong similarity between the quantum and the classical results with the former oscillating around the latter.

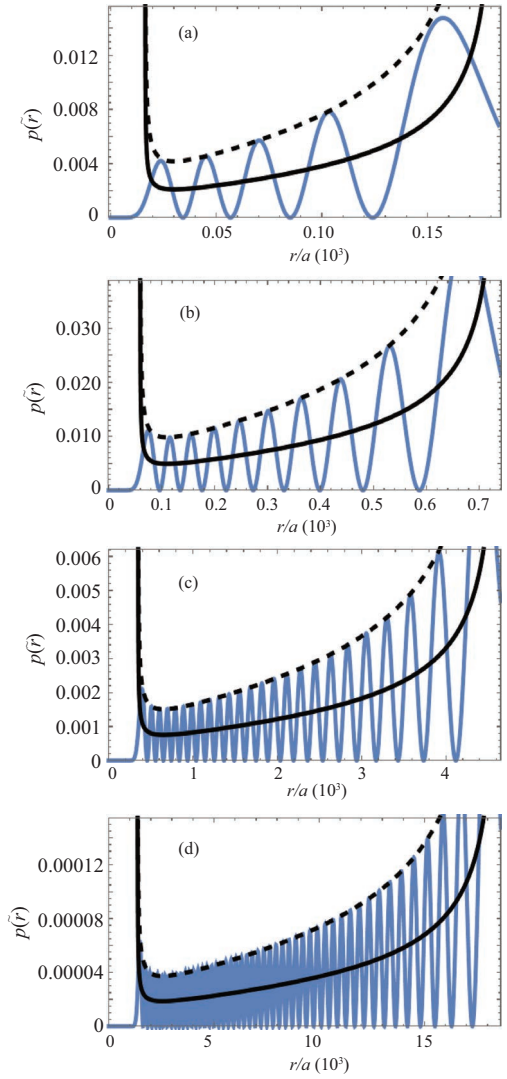


Fig. 6. The radial probability density of hydrogen atom for the case of nonzero angular momentum: (a) $n = 10$, $l = 5$; (b) $n = 20$, $l = 10$; (c) $n = 50$, $l = 25$; (d) $n = 100$, $l = 50$. The ratio l/n is kept at $1/2$. The blue lines are quantum results $p_{\rm q}(\tilde{r})$, the black lines are classical results $p_{\rm c}(\tilde{r})$, and the dashed lines are doubled classical results $2p_{\rm c}(\tilde{r})$.

When the angular momentum is nonzero ($l \neq 0$), the classical orbit is elliptical and has two points where the radial velocity vanishes, leading to divergent radial probability. This is reflected by the fact that Eq. (18) has two singular points at $r_1/a = 2\ell^2/(1-\varepsilon)$ and $r_2/a = \ell^2/(1+\varepsilon)$. As shown in Fig. 6, when n is small, the classical diverging behavior at these two points, in particular, at r_1, is not apparent at all in the quantum probability. However, as n increases, the quantum probability begins to develop sharp peaks around both r_1 and r_2, converging to the classical divergent behavior.

The results presented in both Figs. 5 and 6 clearly demonstrate that the quantum radial probability density converges to its classical counterpart in the limit of $n \to \infty$. These findings support our assertion that the quantum eigenfunction $\psi_{nlm}(\boldsymbol{r})$ can be interpreted as an equal-weight superposition of classical orbits sharing the same energy and angular momentum.

4.2. The angular probability

The quantum angular probability density for hydrogen atom is given by the following expression:

$$\begin{aligned} p_{\rm q}(\theta) &= |\,{\rm Y}_l^m(\theta,\phi)|^2 \sin\theta \\ &= \frac{2l+1}{2}\frac{(l-m)!}{(l+m)!}\,[{\rm P}_l^m(\cos\theta)]^2 \sin\theta, \end{aligned} \tag{26}$$

which is independent of ϕ. Its dependence on $L_z = m\hbar$ is implicit in the form of the associated Legendre function ${\rm P}_l^m(\cos\theta)$. Equation (25) reveals that the classical angular distribution $p_{\rm c}(\theta)$ is also independent of ϕ. Figure 7 compares the quantum and classical angular probability distributions. The figure shows that the trends of the two distributions are similar, and this similarity becomes more pronounced at higher l.

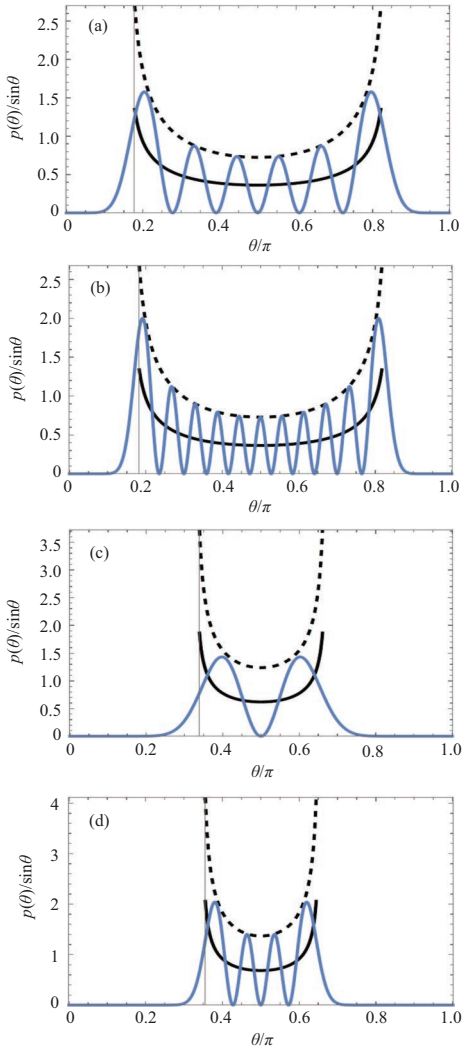


Fig. 7. The angular probability density of hydrogen atom: (a) $l = 10$, $m = 5$; (b) $l = 20$, $m = 10$; (c) $l = 10$, $m = 9$; (d) $l = 30$, $m = 27$. The ratios l/n and m/l are fixed. The blue lines are quantum results $p_{\rm q}(\theta)$, the black solid lines are classical results $p_{\rm c}(\theta)$, and the dashed lines are doubled classical results $2p_{\rm c}(\theta)$.

Together with the results for the radial distribution, we conclude that the energy eigenfunction $\psi_{nlm}(\boldsymbol{r})$ of the hydrogen atom can be regarded as an equal-weight superposition of classical elliptic orbits with energy E_n, angular momentum $L=\sqrt{l(l+1)}\hbar$, and z component of angular momentum $L_z=m\hbar$.

The quantum-classical correspondence that has been established is also evident in a qualitative manner. For both the quantum and classical models of the hydrogen atom, the radial probability density depends solely on quantum numbers n,l , with no dependence on the quantum number m. Similarly, the angular probability density is a function only of l and m, independent of n. The latter observation is particularly insightful because it implies that, although the shape of a single classical orbit is determined by the form of the central force $V(r)$, the overall angular distribution of these classical orbits is independent of the specific form of $V(r)$.

5. Discussion and summary

We have calculated the classical probability densities for the hydrogen atom and compared them with their quantum counterparts. Our findings indicate that, in the semiclassical limit $n\to\infty$, the energy eigenfunction $\psi_{nlm}(\boldsymbol{r})$ of the hydrogen atom can be interpreted as a collection of classical elliptic orbits with energy E_n, angular momentum $L=\sqrt{l(l+1)}\hbar$, and z-component of angular momentum $L_z=m\hbar$.

This serves as a special example of a broader question: What is the classical correspondence of an energy eigenfunction in the semiclassical limit? It is well established that in this limit, an energy eigenfunction reduces to an invariant distribution in classical phase space.[3–5] An ensemble distribution in classical phase space is considered invariant if it remains unchanged over time according to the Liouville equation. This general result can be seen directly via Moyal's equation.[13] For a given wave function $\psi(\boldsymbol{r},t)$, its corresponding Wigner function $W(\boldsymbol{p},\boldsymbol{r},t)$ satisfies Moyal's equation

$$\frac{\partial}{\partial t}W(\boldsymbol{p},\boldsymbol{r},t)=\frac{2}{\hbar}\sin\frac{\hbar}{2}\left[\frac{\partial}{\partial\boldsymbol{p}_W}\frac{\partial}{\partial\boldsymbol{r}_H}-\frac{\partial}{\partial\boldsymbol{p}_H}\frac{\partial}{\partial\boldsymbol{r}_W}\right]H(\boldsymbol{p},\boldsymbol{r})W(\boldsymbol{p},\boldsymbol{r},t),\tag{27}$$

where $\partial/\partial\boldsymbol{p}_W$, $\partial/\partial\boldsymbol{r}_W$ operate only on W and $\partial/\partial\boldsymbol{p}_H$, $\partial/\partial\boldsymbol{r}_H$ only on H. It is evident that in the limit of $\hbar\to0$, the Moyal's equation is reduced to Liouville equation and the Wigner function $W(\boldsymbol{p},\boldsymbol{r},t)$ becomes an ensemble distribution in classical phase space. In particular, when $\psi(\boldsymbol{r},t)$ is an energy eigenfunction, the corresponding Wigner function $W(\boldsymbol{p},\boldsymbol{r})$ is independent of time and becomes an invariant distribution in classical phase space. We define a classical trajectory C as a collection of all the points that a particle traverses in phase space over an infinite long time for a given initial condition. An invariant ensemble must be made of various such trajectories.

With this general result in mind, let us consider a central potential $V(r)$ other than the Coulomb potential. In this case, the orbit may no longer be closed because the radial and angular motion have different periods.[7] Nevertheless, we expect a similar conclusion: the quantum eigenfunction is an equal-weight superposition of all possible classical orbits with the same energy E and the same angular momentum specified by L and L_z. In particular, since the potential $V(r)$ is independent of θ, the angular probability density remains the same and is described by Eq. (25). The radial probability density will be different from Eq. (14) but the classical radial density can be computed similarly as

$$p_{\rm c}(r)=2\frac{\sqrt{(\mathrm{d}r)^2+(r\mathrm{d}\gamma)^2}}{T\,\mathrm{d}r}$$

with T being the period of radial motion.

We expect similar results for a scattering state ($E>0$): in the semiclassical limit, a scattering eigenstate of hydrogen can be viewed as a collection of many unbounded classical orbits with the same energy and the angular momentum. To study such a correspondence, for simplicity, one may first consider a one-dimensional scattering problem. Detailed study of this case is out of scope of this work.

In general, particularly in chaotic systems, the quantum energy eigenfunctions with eigen-energy E_n can still be viewed as a collection of classical orbits with energy E_n. For hydrogen atom or other similar systems, each classical trajectory contributes equally. However, it is an open question how to determine or compute the weight of each classical orbit for a general system.[14]

Appendix A: A classical singularity problem from quantum perspective

Since the 18th century, physicists and mathematicians have grappled with a simple question: What is the fate of a particle initially at rest falling toward a gravitational center? The divergence of the gravitational force at the origin presents a fundamental challenge to classical mechanics, as the equations of motion become singular at $r=0$.[15]

Euler addressed this problem by considering trajectories with small but finite angular momentum L and taking the limit $L\to0$. His analysis suggested the particle would execute a sudden reversal at the center. However, this conclusion sparked considerable debate among his contemporaries. Laplace, for instance, argued that there is a crucial distinction between the limit of flattened elliptical orbits ($L\to0$) and

strictly radial motion. It is much like how a function's limiting behavior may differ from its value at a point. This perspective found support from D'Alembert, who argued for the possibility of the particle passing through the center. Some modern interpretations suggest the particle might halt at the center.[15]

Given the Schrödinger equation has a well-defined solution for a particle at rest falling into a gravitational center, i.e., the case of zero angular momentum $l = 0$, a natural question is whether the quantum-classical correspondence established in the main text could resolve this controversy. Unfortunately, according to the following analysis, the quantum-classical correspondence does not resolve the issue but does provide some new insights.

Since the singularity occurs at $r = 0$, we will proceed to examine how the radial distribution, classical or quantum, behaves in the vicinity of $r = 0$. We first look at the classical radial distribution. In the case of zero angular momentum, i.e., $l = 0$, the distribution is given by Eq. (14), which becomes

$$p_{\rm c}(r) \approx \frac{1}{\pi n^3 a^{3/2}} \sqrt{\frac{r}{2}}, \tag{A1}$$

when $\tilde{r} \to 0$. It is well behaved. In contrast, the radial distribution for $l \neq 0$, given by Eq. (18), diverges at $r_2/a = \ell^2/(1+\varepsilon)$. Specifically, near $\tilde{r} = r_2/a$, the radial distribution for non-zero angular momentum exhibits the following behavior

$$p_{\rm c}(r) \approx \frac{\ell r_2}{2\pi n^3 a^{3/2}} \sqrt{\frac{\varepsilon}{r - r_2}}. \tag{A2}$$

In the classical framework, the angular momentum l is not necessary an integer and can take any positive real number. Consequently, we can consider the limit where l approaches zero. As illustrated in Fig. A1(a), the divergent behavior persists in this limit. In fact, this divergent behavior of the distribution $p_{\rm c}(r)$ is still described by Eq. (A1) with ℓ being a small real number.

The above results indicate that the classical radial distribution $p_{\rm c}(r)$ for non-zero angular momentum ($l \neq 0$), as given by Eq. (18), does not converge to Eq. (14) in the limit where the angular momentum approaches zero ($l \to 0$). This observation suggests that there is indeed a fundamental distinction between motion along an infinitely flattened ellipse and motion along a straight line, thereby lending support to Laplace's assertion.

However, from a different perspective, one might conclude that Euler was correct. Since we are dealing with a probability density function, it is essential to consider how the area under the divergent peak changes as $l \to 0$. The area S under the divergent peak is defined in the inset of Fig. A1(b) and represents the area under the density function between the divergent point and the turning point. As shown in Fig. A1(b), our calculations indicate that the area S tends to zero as $l \to 0$. This implies that, statistically, the peak of the distribution (18) near $r = 0$ can be ignored when l is very small. In this sense, the two density functions (14) and (18) are in agreement in the limit of $l \to 0$. Therefore, we cannot definitively conclude that Laplace was right and Euler was wrong.

Let us now examine whether the quantum radial distribution can provide any new insights into this singularity problem. As illustrated in Fig. 6, the first peak of the quantum radial distribution $p_{\rm q}(r) = |R_{nl}(r)|^2$ diverges in the limit of $l \to \infty$ and $n \to \infty$ while keeping l/n fixed, mirroring the behavior of the classical radial distribution. However, when l is zero, no such divergent behavior is observed, as seen in Fig. 5. Thus, similar to the classical case, the quantum radial distribution for $l \neq 0$ does not approach that for $l = 0$ in the limit of $l \to 0$.

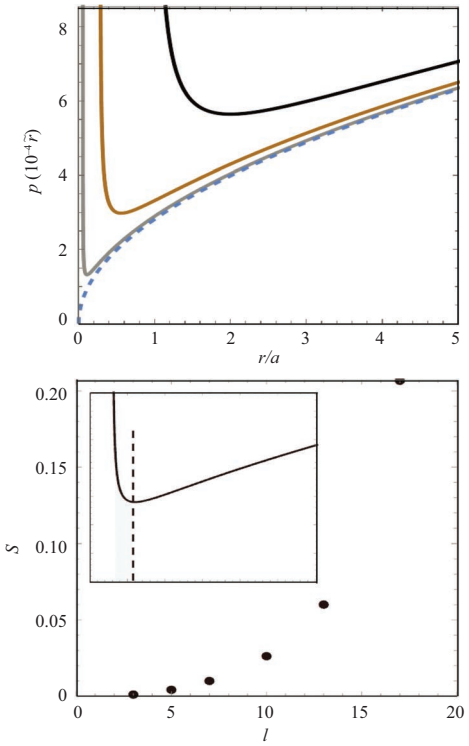


Fig. A1. (a) The radial probability density of the classical hydrogen model for three different values of $l = 1$ (gray), 0.4 (brown), 0.1 (black) at $n = 20$. For comparisons, the density for $l = 0$ is drawn as dashed line. (b) The area of the divergent peak as a function of the angular momentum l at $n = 20$. The inset shows how the area S is defined for a density function. The dashed line in the inset pass the turning point where the derivative of the density function is zero.

To be precise, we need to consider the weight of the diverging peak. For the quantum probability density $p_{\rm q}(r) = |R_{nl}(r)|^2$, the weight of the peak is defined as the area under the function between $r = 0$ and the first peak. The corresponding classical area is defined as the area between the divergent point and the first quantum peak, as shown in the inset of Fig. A2. Note that this classical area is different from the one defined in the inset of Fig. A1; however, they are proportional to each other.

The computed quantum peak areas are shown as a function of n in Fig. A2, along with the classical area. The quantum peak becomes increasingly difficult to compute as n becomes

very large; as a result, we have computed only up to $n = 200$. However, as seen in Fig. A2, the quantum peak area is almost identical to the corresponding classical area. Therefore, we have computed the classical areas for larger n, and the results show that the peak area tends to zero as $n \to \infty$. This indicates that the diverging peak near $r = 0$ in the quantum radial distribution can be statistically ignored.

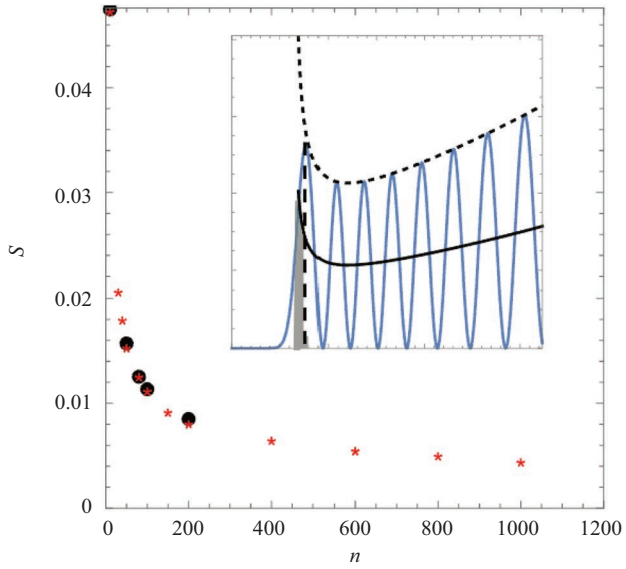


Fig. A2. The quantum peak area S as a function of n. The corresponding classical area is defined in the inset. The quantum results are represented as circles and the classical ones as stars. The computations are done with $l/n = 1/2$ fixed.

In conclusion, the singularity problem of a particle initially at rest falling toward a gravitational center cannot be definitively resolved using distribution functions. On one hand, the diverging behavior of the radial distributions at the limit of $l/n \to 0$ with $n, l \to \infty$ suggests that the particle would make a sudden turn through the gravitational center, supporting Euler's view. However, as the weight of the divergent peak tends to zero, one cannot be entirely certain and rule out Laplace's suggestion that the particle would pass through the center. Nevertheless, we can rule out a recent suggestion that the particle might halt at the center.[15] If the particle halt at the center, we would have a peak of non-zero weight near $r = 0$ for distribution functions.

While our analysis provides some fresh insights, it cannot fully resolve the singularity issue. Our findings indicate that (i) the particle does not remain permanently at the center and (ii) the question of whether Euler's turning-point solution is physically valid remains open. This historical controversy highlights the subtle relationship between limiting processes and physical reality, a theme that recurs throughout mathematical physics.

Acknowledgment

Project supported by the National Natural Science Foundation of China (Grant Nos. 92365202, 12475011, and 11921005), the National Key Research and Development Program of China (Grant No. 2024YFA1409002), the Shanghai Municipal Science and Technology Major Project (Grant No. 2019SHZDZX01), the Shanghai Municipal Science and Technology Project (Grant No. 25LZ2601100), and the Innovation Program for Quantum Science and Technology (Grant No. 2021ZD0302100).

References

[1] Pauling L and Wilson E B 1935 *Introduction to Quantum Mechanics* (New York: McGraw-Hill) p. 76
[2] Leubner C, Alber M and Schupfer N 1988 *Am. J. Phys.* **56** 1123
[3] Berry M 1977 *J. Phys. A: Math, Gen.* bf 10 2038
[4] Berry M 1983 *Semiclassical mechanics of regular and irregular motion*, in *Les Houches Lecture Series Session XXXVI*, eds. Iooss G, Helleman R H G and Stora R (Amsterdam: North Holland) pp. 171–271
[5] Zhang Z, Wang Z and Wu B 2023 *Phys. Rev. E* **107** 034123
[6] Abrines R and Percival I C 1966 *Proc. Phys. Soc.* **88** 861
[7] Li X K, Wang C C, Yuan Z Q, Ye D F, Ma P, Hu W H, Luo S Z, Fu L B and Ding D J 2017 *Phys. Rev. A* **96** 033416
[8] Cui E and Ye D 2025 *Chin. Phys. B* **34** 073201
[9] Lui S, Ye D and Liu J 2023 *Chin. Phys. B* **32** 063402
[10] Griffiths D J and Schroeter D F 2018 *Introduction to Quantum Mechanics* (Cambridge: Cambridge University Press)
[11] Robnik M and Salasnich L 1997 *J. Phys. A: Math. Gen.* **30** 1719
[12] Goldstein H 2002 *Classical Mechanics* (Massachusetts: Addison-Wesley)
[13] Moyal J E 1949 *Math. Proc. Camb. Philos. Soc.* **45** 99
[14] Kong L, Gong Z and Wu B 2024 *Phys. Rev. E* **109** 054113
[15] Gapaillard J 2018 *Le trou noir des Lumieres* (Paris: Pour La Science) pp. 80–85